Mo et al. Nanoscale Research Letters (2016) 11:354
DOI 10.1186/s11671-016-1566-7

Nanoscale Research Letters

NANO EXPRESS Open Access

Influence of Thickness on the Electrical Transport Properties of Exfoliated Bi_2Te_3 Ultrathin Films

D. L. Mo[1,2], W. B. Wang[1,2] and Q. Cai[1,2*]

Abstract

In this work, the mechanical exfoliation method has been utilized to fabricate Bi_2Te_3 ultrathin films. The thickness of the ultrathin films is revealed to be several tens of nanometers. Weak antilocalization effects and Shubnikov de Haas oscillations have been observed in the magneto-transport measurements on individual films with different thickness, and the two-dimensional surface conduction plays a dominant role. The Fermi level is found to be 81 meV above the Dirac point, and the carrier mobility can reach ~6030 $cm^2/(Vs)$ for the 10-nm film. When the film thickness decreases from 30 to 10 nm, the Fermi level will move 8 meV far from the bulk valence band. The coefficient α in the Hikami-Larkin-Nagaoka equation is shown to be ~0.5, manifesting that only the bottom surface of the Bi_2Te_3 ultrathin films takes part in transport conductions. These will pave the way for understanding thoroughly the surface transport properties of topological insulators.

Keywords: Bi_2Te_3 ultrathin films, Exfoliation, Thickness influence, Weak antilocalization, Shubnikov de Haas oscillations

Background

As a unique class of condense matter materials, topological insulators (TIs) have attracted considerable attention these years for their potential applications in spintronics and quantum computation [1, 2]. TIs are characterized by intrinsic insulating bulk states and metallic surface states due to strong spin-orbit coupling. Theoretically, the Dirac-like surface states of TIs are protected by charge symmetry and time reversal invariance, to guarantee it non-trivial. As a result, the electron spin is locked with its momentum and the backscattering induced by nonmagnetic impurities is prohibited. These special natures of TIs bring forth exotic phenomena, such as quantum spin Hall effect and Majorana fermions appearing in vortex cores between the interface of TI and superconductor [1–4]. After HgTe/CdTe quantum wells, Bi_2Se_3, Bi_2Te_3, and Sb_2Te_3 as the second generation of three-dimensional TIs were proved with angle-resolved photoemission spectroscopy (ARPES) experiments to have the surface states exhibiting ideal single Dirac cone in energy band structures [5–7]. In recent years, mesoscopic quantum interference phenomena of these TI materials have been heatedly researched, such as Aharonov-Bohm oscillations, universal conductance fluctuations, weak antilocalization (WAL) effects and Shubnikov de Haas (SdH) oscillations, in which many relevant physical parameters have been obtained [8–13].

It is well-established that bismuth-telluride (Bi_2Te_3) is an important thermoelectric material. After confirmed as TI with very strong spin-orbit coupling, Bi_2Te_3 becomes a proper platform for investigating WAL effects. The current researches usually focus on Bi_2Se_3, which has a relatively large band gap in bulk (~0.3 eV). The Bi_2Se_3 and Bi_2Te_3 samples are commonly fabricated through chemical solution synthesis, molecular beam epitaxy, and chemical vapor deposition [10, 14, 15]. To utilize surface states of TI, the Fermi level of surface states must be near the Dirac point. The chemical nature of graphene ensures that the Fermi level is located naturally at the Dirac point, but it is not the case for TIs [1]. And there is a major hindrance for researching the exotic

* Correspondence: qcai@fudan.edu.cn
[1]State Key Laboratory of Surface Physics and Department of Physics, Fudan University, Shanghai 200433, China
[2]Collaborative Innovation Center of Advanced Microstructures, Nanjing 210093, China

transport properties of TI surface states. The conducting bulk is usually more prevalent due to the existence of vacancies and impurities. Therefore, it is difficult to control and manipulate independently the conduction from the topological surface/edge states [16]. In order to suppress the bulk contributions to electrical transport and focus on the transport properties of surface states, two solutions can be employed: to manipulate the Fermi level by elemental doping/electric gating or to increase the surface-to-volume ratio. The ARPES and Hall transport experiments on Bi_2Se_3 showed that a small amount of Ca doping would result in insulating bulk, and the resistivity of the TI samples could be easily affected by Ca concentration [17]. It was found that the bulk conductance was suppressed by four orders of magnitude in the Cu doped Bi_2Te_3 films [18]. When the thickness of TI films is decreased to nanoscale or the nanostructures of TI materials are constructed, the surface-to-volume ratio of the samples will become larger. And the contributions from the topological surface conduction will dominate the transport properties [19, 20].

It is well-known that Bi_2Te_3 has a layered crystal structure, and the weak van der Waals interaction exists between its atomic quintuple layers [21, 22]. Therefore, Bi_2Te_3 can be exfoliated into ultrathin films with the thickness even down to several quintuple layers. In recent years, the transport properties of Bi_2Te_3 films have been studied widely. However, the explicit experimental investigations about the influence of the film thickness have not been reported on the electron transport of gapless surface states within our knowledge. The systematic explorations about thickness effects of TI thin films will be useful and compatible to device fabrication. In this work, the Bi_2Te_3 ultrathin films are prepared by means of mechanical exfoliation. The film thickness is manifested ranging from 10 to 200 nm by using scanning electron microscopy, atomic force microscopy, and Raman spectroscopy, as well as its relations with the size. The relevant transport parameters have been obtained from the measurements of WAL effects and SdH oscillations, and the influences of film thickness are discussed on the transport properties of gapless surface states. It is shown that there is only the bottom surface participating in the observed WAL conduction for the Bi_2Te_3 films as thin as 10 nm. The present results can provide a valuable insight into the applications of TIs in future electronic and spintronic devices.

Methods

Owing to the layered crystal structure, the Bi_2Te_3 ultrathin films were produced by means of mechanical exfoliation from the commercial crystalline bulk Bi_2Te_3 with a purity of 99.99 %. After exfoliation, the obtained micro-flakes of Bi_2Te_3 were transferred onto a Si substrate with a 285-nm SiO_2 layer on the surface. The morphology and thickness of Bi_2Te_3 ultrathin films were characterized mainly with scanning electron microscopy (SEM), atomic force microscopy (AFM), and micro-Raman spectroscopy. SEM experiments were performed in a Zeiss Sigma SEM system with Raith Elphy Plus, which functioned at 5 kV for topography observation and 20 kV for electron beam lithography. The AFM observations were carried out in air using noncontact mode, and Raman spectra were obtained with a laser excitation at 632 nm. In order to investigate the electrical transport properties, the four-terminal contacts were fabricated for a single Bi_2Te_3 ultrathin film on the SiO_2/Si substrate by using electron beam lithography followed by the 5 nm/50 nm Cr/Au metal depositions with an electron beam evaporator and lift-off process. The electrical transport measurements were carried out, with the temperature ranging from 2 to 300 K and a magnetic field perpendicular to the sample plane, in a quantum design physical property measurement system under the pressure of 10 torr. The standard four-probe technique for transport measurements was adopted to eliminate the effects of contact resistance, with the two outer electrodes connected to a current source and the two inner electrodes to a voltmeter.

Results and Discussion

In order to roughly know about the distributions of Bi_2Te_3 micro-flakes on the SiO_2/Si substrate, the optical microscopy and SEM observations were performed. It is found that the thinner the micro-flake is, the darker its color will be under the optical microscope. And the size and surface morphology of the micro-flakes can be obtained in detail in the SEM images. It is shown that the micro-flakes have very smooth surfaces with the step-shaped edges, and their sizes can reach tens of micrometers, much larger than those of the Bi_2Te_3 nanoplates synthesized in chemical methods [10]. The precise information about the thickness of Bi_2Te_3 micro-flakes can be acquired in the AFM measurements. Their thickness is demonstrated varying from a few nanometers to several hundred nanometers, as shown in Table 1. It can be seen that the thickness of Bi_2Te_3 micro-flakes increases with the increasing size, unlike that of graphene exfoliated from graphite, in which van der Waals's force is much smaller than that in Bi_2Te_3.

Table 1 Size and thickness of Bi_2Te_3 micro-flakes obtained from SEM and AFM observations

Size (μm)	1–5	5–10	10–20	20–50	>50
Thickness (nm)	10–15	15–30	30–70	70–200	>200

For bulk Bi_2Te_3, it is known that its crystal structure belongs to space group R 3m (D_{3d}^5). And in one unit cell, five atomic layers can be discerned, which commonly called a quintuple [21]. In Raman spectra of Bi_2Te_3, the most distinct features are E_g^2 peak (E^2) at ~103 cm^{-1} and A_{1g}^2 peak (A^2) at ~133 cm^{-1}. It is also reported that the intensity ratios of the E_g^2 peak to the A_{1g}^2 peak can be used to evaluate the thickness of Bi_2Te_3 films [23]. The A_{1u} peak at ~117 cm^{-1} which is not Raman active in bulk can also emerge when the thickness of Bi_2Te_3 film is less than 40 nm, and it will become more and more obvious with the decreasing of the film thickness due to crystal-symmetry breaking [21, 23].

Figure 1 is Raman spectra of the exfoliated Bi_2Te_3 ultrathin films with different thickness measured at room temperature. There are mainly two peaks, E^2 at 101 cm^{-1} and A^2 at 133 cm^{-1}, excited with a 632-nm laser. The sharpness of the peaks indicates that the crystal quality of the ultrathin films is great, and the films have very few impurities and defects inside. The intensity ratios $I(E^2)/I(A^2)$ for the ultrathin films at different thickness are shown in Table 2. It is displayed clearly that the ratio decreases with the decrease of the film thickness, in agreement with the previous work [23]. Because of the out-of-plane symmetry (perpendicular to the quintuple layers) no longer existing, the out-of-plane vibration mode (A^2) can be highlighted in the Bi_2Te_3 ultrathin films. With the decreasing of the thickness, the E^2 and A^2 peaks are found in Fig. 1 slightly red-shifted, owing to the bending of the ultrathin films and the consequent strain. However, the $I(E^2)/I(A^2)$ ratios in our work are much larger than those measured in the previous work [23]. It is also surprising that the A_{1u} peak at ~117 cm^{-1} cannot be observed in our Raman spectra even if the thickness of the Bi_2Te_3 films is as thin as 15 nm. In Fig. 1, it is distinctly exhibited that the 15-nm film is so gauzy that the Si-Si peak from the substrate (280–350 cm^{-1}) can also be detected. No reasonable explanations can be given right now, although a laser light of 488 nm has been noticed to be used in the previous works [21, 23].

For the investigations to electrical transport properties of the exfoliated Bi_2Te_3 ultrathin films, the standard four-terminal geometry devices were fabricated on the samples *via* electron beam lithography. As shown in Fig. 2, the resistance of the ultrathin film was measured as a function of temperature ranging from 2 to 300 K. A typical optical image of the exfoliated film is exhibited in the inset of Fig. 2 after the preparation of the electrodes. It can be seen that the film is almost transparent under optical microscope, on account of its extreme thinness. The right inset shows the details in the area marked by a square in Fig. 2.

Because of the tellurium vacancies or impurities existing, Bi_2Te_3 usually exhibits very good electrical conductivity. In Fig. 2, the resistance of Bi_2Te_3 ultrathin film presents principally a metallic behavior, consistent with the previous works [8, 9]. It can be seen that the resistance increases with the temperature increasing at the range of 10 to 300 K, implying that conductivity is dominated by the carrier mobility. As the temperature decreases, the phonon scattering reduces, resulting in the carrier mobility increasing and the resistance decreasing. When the temperature T lowers below 10 K, the resistance is found to increase with T dropping and appears

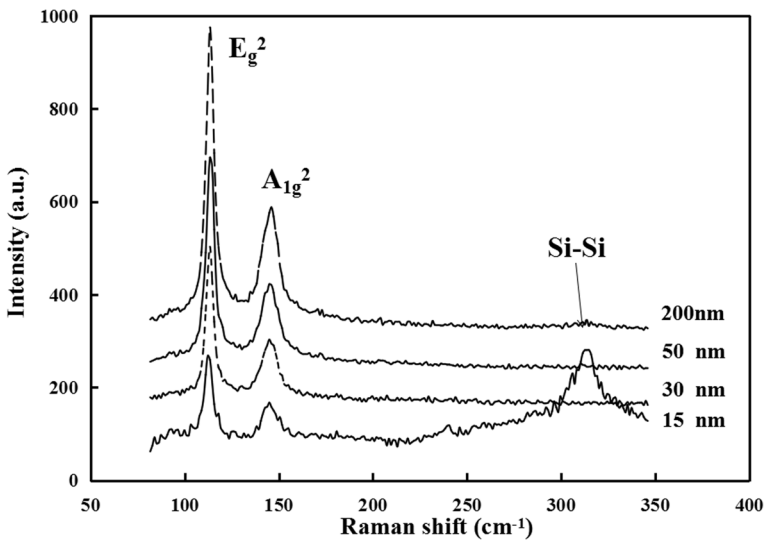

Fig. 1 Raman spectra of the exfoliated Bi_2Te_3 ultrathin films with different thickness

Table 2 The intensity ratios of E^2 to A^2 Raman peak at different film thickness

Thickness (nm)	200	50	30	15
I (E^2)/I (A^2)	3.33	2.84	2.67	2.50

to present *ln*T dependence below 5 K as shown in the right inset of Fig. 2, presumably due to freezing effect of the carriers, electron-electron interactions and WAL effect [24, 25]. The low temperature less than 10 K usually brings about the absence of inelastic phonon scattering [8], and impurity scattering of the charge carriers should dominate the transport [26]. This impurity scattering substantially does not change with temperature. However, the temperature dropping causes the carrier concentration to diminish, resulting in the resistance increasing. When T drops below 5 K, electron-electron interactions as well as WAL effect probably make important contributions to conduction, at last inducing the *ln*T dependence of resistance [25]. In addition, the semiconductor-like resistance below 10 K shown in Fig. 2 indicates that bulk conductance of Bi_2Te_3 ultrathin films is suppressed to a large extent, and surface conduction will act as a non-negligible role [24].

The magneto-transport properties of individual Bi_2Te_3 ultrathin film were investigated with the magnetic field B perpendicular to the ultrathin film. Figure 3a shows the magneto-conductance G plotted as a function of B obtained at 2 K on four samples with the thickness of 10, 15, 30, and 50 nm, respectively. Figure 3b shows the magneto-conductance acquired at different temperature on the 10-nm sample. It is clear to see in Fig. 3a, b that there are dips near $B = 0$ T, the prominent feature for the

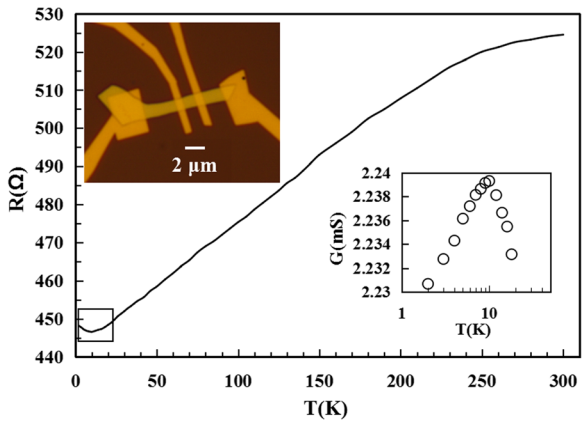

Fig. 2 The measured resistance of the Bi_2Te_3 ultrathin film with a thickness of 15 nm is plotted as a function of temperature. The *left inset* shows a typical optical image of the four-terminal electrodes fabricated on a single ultrathin film. The *right inset* illustrates the details in the area marked by a square

WAL effect. The WAL cusp persists to the temperature of 10 K. And at 20 K, the G-B curve exhibits a parabolic dependence at small field which is typical for metallic transport of the bulk states due to the Lorentz deflection [18]. The WAL effect can be described by a simplified Hikami-Larkin-Nagaoka (HLN) equation [27]:

$$\Delta G(B) = -\frac{\alpha e^2}{\pi h}\left[\Psi\left(\frac{1}{2}+\frac{h}{8e\pi L_\phi{}^2 B}\right)-\ln\left(\frac{h}{8e\pi L_\phi{}^2 B}\right)\right] \quad (1)$$

Here, $\Delta G(B) = G(B) - G(0)$ is the change of magneto-conductance, $\Psi(x)$ is the digamma function, α is a coefficient indicating the type of localization, L_ϕ is the phase coherent length, h is the Planck constant, and e is electronic charge. According to Fig. 3, the experimental data are fitted with the HLN equation and $\alpha = 0.47$ is obtained for the Bi_2Te_3 ultrathin film of 10 nm at 2 K, quite close to the theoretical value of 0.5 for WAL in a single conductive channel.

The fitting parameter α is ~0.5 here, manifesting that there is only one topological surface contributing to the WAL transport for our exfoliated Bi_2Te_3 films. And presumably, it is the bottom surface of the ultrathin films that dominates the conduction, due to oxidation and photolithographic contaminations existing on the top surface [10]. In Fig. 3c, d, the parameters of α and L_ϕ extracted from the HLN fittings are plotted as the function of thickness and temperature, respectively. It is shown that α deviates from 0.5 to some extent with the increasing of film thickness, suggesting the bulk contribution to transport becoming larger and disturbing the signal from the surface states. A similar trend happens for α with the increasing of temperature. The phase coherent length L_ϕ is also displayed to decrease with the film thickness increased, due to the effects of the surface states on conduction lowered. L_ϕ can reach 188 nm for the 10-nm film. In Fig. 3d, it is noted that L_ϕ can be fitted well with the $T^{-1/2}$ dependence at the temperature ranging from 2 to 20 K, indicating again that electron-electron interactions become a significant source of dephasing [28]. The $T^{-1/2}$ dependence of L_ϕ is a typical characteristic of two-dimensional electron interference [18], and it gives evidence of the electrical transport through topological surface states existing in the 10-nm Bi_2Te_3 ultrathin film.

When a material with high carrier mobility stays in a magnetic field B, the SdH oscillations will be usually observed, in which the magneto-resistance R varies periodically with 1/B due to consecutive emptying of Landau levels with the increasing of the magnetic field [29, 30]. From the R-B curves obtained experimentally at 2 K with the background subtracted, the SdH

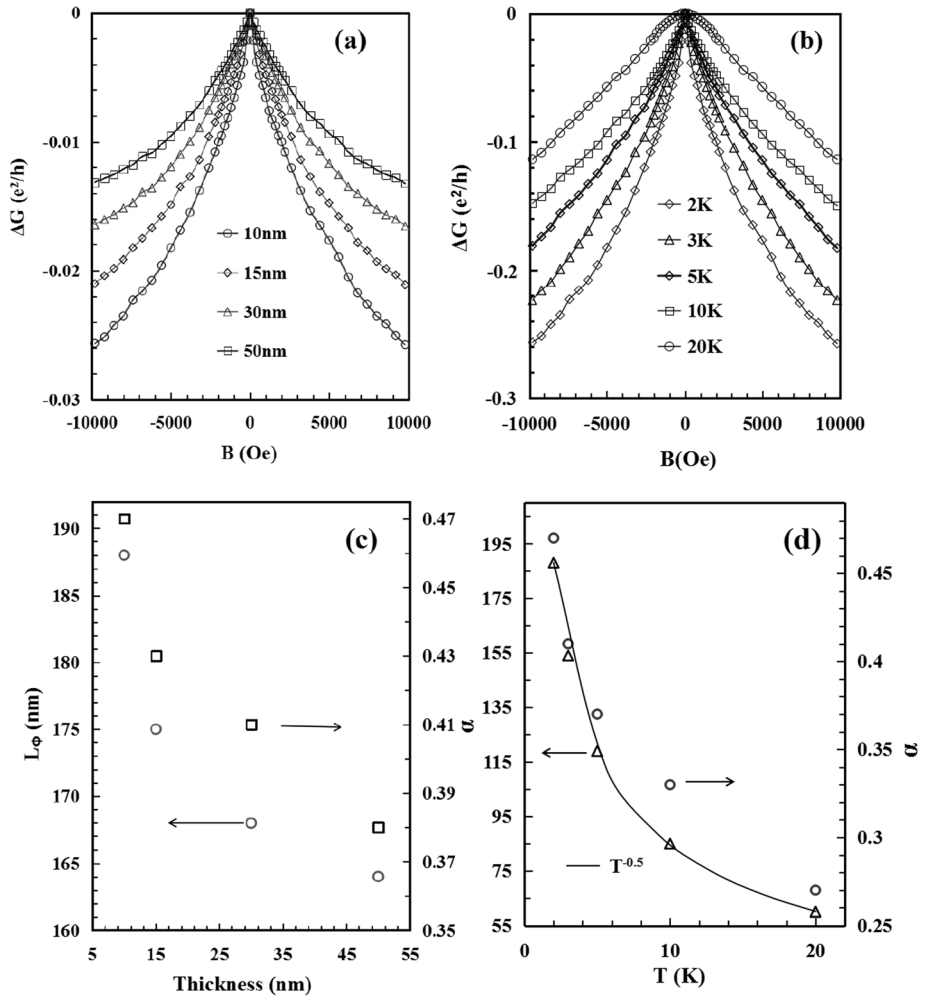

Fig. 3 **a** The magneto-conductance obtained at 2 K on the Bi_2Te_3 films with different thickness. **b** The magneto-conductance curves acquired at different temperature on a 10-nm Bi_2Te_3 film. **c**, **d** The phase coherent length L_φ and the coefficient α are shown versus thickness and temperature, respectively. The solid line in (**d**) is the $T^{-1/2}$ fitting of L_φ

oscillations are definitely shown in Fig. 4a for the Bi_2Te_3 ultrathin films with different thickness. It can be found that the oscillation amplitude decreases with the increasing of thickness, implying that the surface conduction plays a major role in the SdH oscillations for the ultrathin film. And then, the oscillations are molested by the bulk transport of the thick film, where the universal conductance fluctuations come to be more pronounced. By using fast Fourier transform, the oscillation frequency will be achieved as $f_{SdH} = 41.2$ T for the 10-nm film. Since the period of SdH oscillations $\Delta(1/B) = 4\pi e/(\hbar k_F^2)$ [8], the frequency $f_{SdH} = \hbar k_F^2/(4\pi e)$ and the extremal cross-sectional area of the Fermi surface $S_F = \pi k_F^2$, then the Fermi vector k_F is obtained as 0.35/nm. The cyclotron mass can be determined according to the T dependence of the amplitude $\Delta\sigma_{xx}$ of conductivity oscillations: $\Delta\sigma_{xx}(T) = \Delta\sigma_{xx}(0)\ \lambda(T)/sinh\lambda(T)$. For the surface states, the thermal factor λ(T) is given by

$$\lambda(T) = 2\pi^2 k_B T m_{cyc}/(\hbar eB) \quad (2)$$

Here k_B is Boltzmann's constant and m_{cyc} is the cyclotron mass [31–33]. Figure 4b shows the normalized conductivity amplitudes $\Delta\sigma_{xx}(T)$ plotted as the function of temperature for the ultrathin films with different thickness. It is found that $m_{cyc} = 0.117\ m_0$ (m_0 is the electron rest mass) by fitting the T dependence of the amplitude $\Delta\sigma_{xx}(T)$ to Eq. (2). Note that $m_{cyc}V_F = \hbar k_F$; therefore, the Fermi velocity $V_F = \hbar k_F/m_{cyc} = 3.47 \times 10^5$ m/s and the Fermi level $E_F = m_{cyc}V_F^2 = 81$ meV above the Dirac point for the 10-nm Bi_2Te_3 film. The lifetime τ of the surface

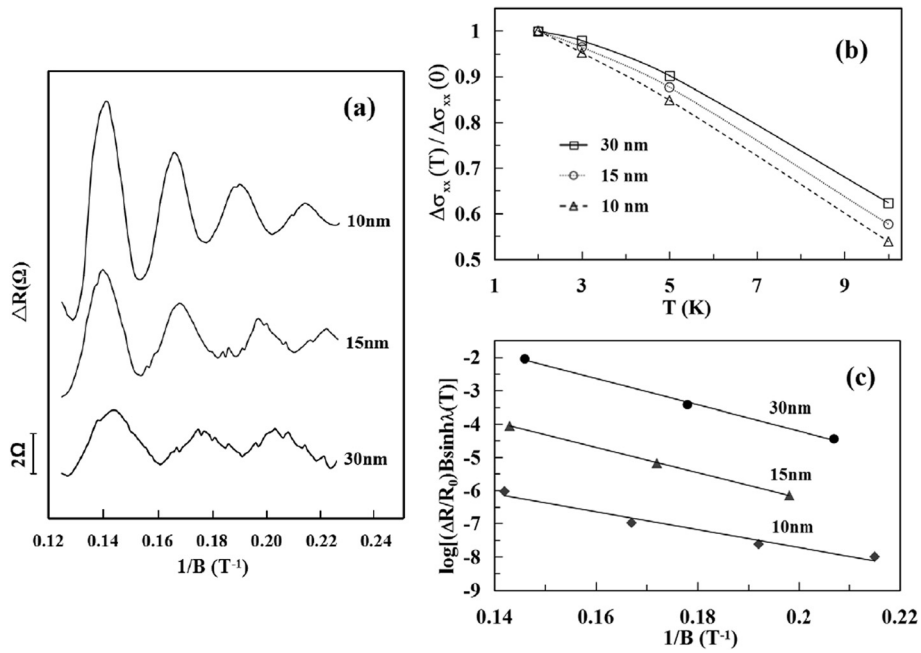

Fig. 4 **a** The SdH oscillations obtained at 2 K on the Bi_2Te_3 films with thickness of 10, 15, and 30 nm, respectively. **b** The corresponding conductivity amplitudes are plotted as the function of temperature. **c** The Dingle plots at 2 K of the films with different thickness

states can be obtained by estimating the Dingle factor e^{-D}, where $D = 2\pi^2 E_F/(\hbar e B \tau V_F^2)$ [24, 31, 33]. Because the amplitude of resistance oscillation $\Delta R/R_0 \sim [\lambda(T)/\sinh\lambda(T)]e^{-D}$ [24, 31], τ can be found from the slope in the plot of $\log(\Delta R/R_0)B\sinh\lambda(T)$ versus 1/B (shown in Fig. 4c). Then the carrier lifetime $\tau = 4.01 \times 10^{-13}$ s, and the carrier mobility $\mu = e\tau/m_{cyc} = 6030$ $cm^2/(Vs)$ for the 10 nm film, seven times larger than the bulk mobility $\mu_b \sim 860$ $cm^2/(Vs)$ [31]. For the experimental data obtained on the films with different thickness at 2 K, the parameters shown in Table 3 can be achieved.

For the exfoliated Bi_2Te_3 ultrathin films, the Fermi level is about 80 meV above the Dirac cone, consistent with the previous work [24]. With the thickness decreasing from 30 to 10 nm, the Fermi level moves 8 meV far from the Dirac point and the bulk valence band. According to the band structures of Bi_2Te_3 [6], it is testified that the Fermi level of our exfoliated Bi_2Te_3 ultrathin films shifts into the bulk gap, and the electrical transport properties are dominated by topological surface states for the Bi_2Te_3 films with very small thickness. Balandin et al. have explored the thickness dependence for the resistance and thermoelectric efficiency of the exfoliated Bi_2Se_3 and Bi_2Te_3 films [34, 35], and it is also revealed that the surface transport through the topological surface states will play more and more predominant roles with the film thickness decreased. According to Ref. [19], the mobility of Bi_2Te_3 films obtained with molecular beam epitaxy (MBE) growth is 521 $cm^2/(Vs)$. The mobility of our samples fabricated by means of mechanical exfoliation can reach 6030 $cm^2/(Vs)$, much higher than those of the samples obtained in MBE growth [28] and chemical method [24]. Probably because the samples in the previous works have a non-insulating substrate or a surface/crystal structure not so intact as those of our exfoliated samples. In this work, the experimental mobility of carriers is found in the range of 5680 to 6030 $cm^2/(Vs)$, increasing with the thickness decreased and diminishing with the bulk transport involved. It is proposed that ultra-small thickness for TIs is a good way to control and suppress the bulk contribution to the electrical transport.

Conclusions

In summary, the Bi_2Te_3 ultrathin films with the thickness of several tens of nanometers have been fabricated

Table 3 The estimated transport parameters from SdH oscillations observed at 2 K on the Bi_2Te_3 films with different thickness

t (nm)	f_{SdH} (T)	k_F (nm^{-1})	m_{cyc} (m_0)	V_F (10^5 ms^{-1})	E_F (meV)	τ (10^{-13} s)	μ (cm^2V^{-1} s^{-1})
10	41.2	0.35	0.117	3.47	81	4.01	6030
15	35.3	0.33	0.107	3.51	77	3.61	5840
30	31.5	0.31	0.101	3.55	73	3.27	5680

by using mechanical exfoliation. According to the experimental results of SEM, AFM, and Raman Spectroscopy, the ultrathin films are found to possess excellent crystal quality as well as smooth surfaces, and their thickness increases with the increasing of size. The WAL effect and SdH oscillations have been observed in the magneto-transport investigations for the films with magnetic field perpendicular to the surface. It is verified that the two-dimensional transport through topological surface states plays a dominant role in conductance of the film as thin as 10 nm. The coefficient α in the HLN equation has a measurement of ~0.5 and suggests that only one surface channel contributes to the conduction. It is shown that the carrier mobility can reach ~6000 $cm^2/(Vs)$ for the thinner film, almost one order of magnitude larger than the bulk mobility. Ultra-small thickness is demonstrated an effective way for TIs to control and suppress the bulk contribution to transport.

Competing interests
The authors declare that they have no competing interests.

Authors' contribution
DLM carried out the mechanical exfoliations, microscope observations, Raman and transport measurements, and he drafted the manuscript. WBW participated in the exfoliations, SEM observations and Raman measurements. QC designed the experiments and drafted the manuscript. All authors read and approved the final manuscript.

Acknowledgements
The authors would like to acknowledge the experimental assistance and helpful suggestions from Dr. Yijun Yu and Prof. Yuanbo Zhang, Department of Physics of Fudan University. This work was supported by the National Natural Science Foundation of China under Grant No. 11374058 and the National Science Fund for Talent Training in Basic Science under Grant No. J1103204.

Received: 20 April 2016 Accepted: 26 July 2016
Published online: 02 August 2016

References
1. Hasan MZ, Kane CL (2010) Colloquium: Topological insulators. Rev Mod Phys 82:3045
2. Kong DS, Cui Y (2011) Opportunities in chemistry and materials science for topological insulators and their nanostructures. Nat Chemistry, 3:845
3. Fu L, Kane CL (2008) Superconducting proximity effect and Majorana fermions at the surface of a topological insulator. Phys Rev Lett 100:096407
4. Freedman MH, Larsen M, Wang Z (2002) A modular functor which is universal for quantum computation. Commun Math Phys 227:605
5. Xia Y, Qian D, Hsieh D, Wray L, Pal A, Lin H, Bansil A, Grauer D, Hor YS, Cava RJ, Hasan MZ (2009) Observation of a large-gap topological-insulator class with a single Dirac cone on the surface. Nat Phys 5:398
6. Chen YL, Analytis JG, Chu JH, Liu ZK, Mo SK, Qi XL, Zhang HJ, Lu DH, Dai X, Fang Z, Zhang SC, Fisher IR, Hussain Z, Shen ZX (2009) Experimental realization of a three- dimensional topological insulator, Bi_2Te_3. Science 325: 178
7. Hsieh D, Xia Y, Qian D, Wray L, Meier F, Dil JH, Osterwalder J, Patthey L, Fedorov AV, Lin H, Bansil A, Grauer D, Hor YS, Cava RJ, Hasan MZ (2009) Observation of time-reversal-protected single-Dirac-cone topological-insulator states in Bi_2Te_3 and Sb_2Te_3. Phys Rev Lett 103:146401
8. Peng HL, Lai KJ, Kong DS, Meister S, Chen YL, Qi XL, Zhang SC, Shen ZX, Cui Y (2010) Aharonov-Bohm interference in topological insulator nanoribbons. Nat Materials 9:225
9. Chen J, Qin HJ, Yang F, Liu J, Guan T, Qu FM, Zhang GH, Shi JR, Xie XC, Yang CL, Wu KH, Li YQ, Lu L (2010) Gate-voltage control of chemical potential and weak antilocalization in Bi_2Se_3. Phys Rev Lett 105: 176602
10. Wang Y, Xiu FX, Cheng L, He L, Lang MR, Tang JS, Kou XF, Yu XX, Jiang XW, Chen ZG, Zou J, Wang KL (2012) Gate-controlled surface conduction in Na-doped Bi_2Te_3 topological insulator nanoplates. Nano Lett 12:1170
11. Li ZG, Chen TS, Pan HY, Song FQ, Wang BG, Han JH, Qin YY, Wang XF, Zhang R, Wan JG, Xing DY, Wang GH (2012) Two-dimensional universal conductance fluctuations and the electron-phonon interaction of surface states in Bi_2Te_2Se microflakes. Sci Rep 2:595
12. Hamdou B, Gooth J, Dorn A, Pippel E, Nielsch K (2013) Aharonov-Bohm oscillations and weak antilocalization in topological insulator Sb_2Te_3 nanowires. Appl Phys Lett 102:223110
13. Liao J, Ou YB, Feng X, Yang S, Lin CJ, Yang WM, Wu KH, He K, Ma XC, Xue QK, Li YQ (2015) Observation of Anderson localization in ultrathin films of three-dimensional topological insulators. Phys Rev Lett 114: 216601
14. Wang K, Liu YW, Wang WY, Meyer N, Bao LH, He L, Lang MR, Chen ZG, Che XY, Post K, Zou J, Basov DN, Wang KL, Xiu FX (2013) High-quality Bi_2Te_3 thin films grown on mica substrates for potential optoelectronic applications. Appl Phys Lett 103:031605
15. Tang H, Liang D, Qiu RLJ, Gao XPA (2011) Two-dimensional transport-induced linear magneto-resistance in topological insulator Bi_2Se_3 nanoribbons. ACS Nano 5:7510
16. Hong SS, Cha JJ, Kong DS, Cui Y (2012) Ultra-low carrier concentration and surface-dominant transport in antimony-doped Bi_2Se_3 topological insulator nanoribbons. Nat Commun 3:757
17. Hsieh D, Xia Y, Qian D, Wray L, Dil JH, Meier F, Osterwalder J, Patthey L, Checkelsky JG, Ong NP, Fedorov AV, Lin H, Bansil A, Grauer D, Hor YS, Cava RJ, Hasan MZ (2009) A tunable topological insulator in the spin helical Dirac transport regime. Nature 460:1101
18. Chen TS, Chen Q, Schouteden K, Huang WK, Wang XF, Li Z, Miao F, Wang XR, Li ZG, Zhao B, Li SC, Song FQ, Wang JL, Wang BG, van Haesendonck C, Wang GH (2014) Topological transport and atomic tunneling-clustering dynamics for aged Cu-doped Bi_2Te_3 crystals. Nat Commun 5:5022
19. He HT, Wang G, Zhang T, Sou IK, Wong GKL, Wang JN, Lu HZ, Shen SQ, Zhang FC (2011) Impurity effect on weak antilocalization in the topological insulator Bi_2Te_3. Phys Rev Lett 106:166805
20. Wang LX, Yan Y, Liao ZM, Yu DP (2015) Gate-modulated weak antilocalization and carrier trapping in individual Bi_2Se_3 nanoribbons. Appl Phys Lett 106:063103
21. Teweldebrhan D, Goyal V, Balandin AA (2010) Exfoliation and characterization of bismuth telljuride atomic quintuples and quasi-two-dimensional crystals. Nano Lett 10:1209
22. Teweldebrhan D, Goyal V, Rahman M, Balandin AA (2010) Atomically-thin crystalline films and ribbons of bismuth telluride. Appl Phys Lett 96:053107
23. Shahil KMF, Hossain MZ, Teweldebrhan D, Balandin AA (2010) Crystal symmetry breaking in few-quintuple Bi_2Te_3 films: applications in nanometrology of topological insulators. Appl Phys Lett 96:153103
24. Xiu F, He L, Wang Y, Cheng L, Chang LT, Lang M, Huang G, Kou X, Zhou Y, Jiang X, Chen Z, Zou J, Shailos A, Wang KL (2011) Manipulating surface states in topological insulator nanoribbons. Nat Nanotech 6:216
25. Li Y, Wu K, Shi J, Xie X (2012) Electron transport properties of three-dimensional topological insulators. Front Phys 7:165
26. Conwell E, Weisskopf VF (1950) Theory of impurity scattering in semiconductors. Phys Rev 77:388
27. Hikami S, Larkin AI, Nagaoka Y (1980) Spin-orbit interaction and magnetoresistance in the two dimensional random system. Prog Theor Phys 63:707
28. Dey R, Pramanik T, Roy A, Rai A, Guchhait S, Sonde S, Movva HCP, Colombo L, Register LF, Banerjee SK (2014) Strong spin-orbit coupling and Zeeman spin splitting in angle dependent magnetoresistance of Bi_2Te_3. Appl Phys Lett 104:223111
29. Schoenberg D (1984) Magnetic Oscillations in Metals. Cambridge University Press, Cambridge
30. Bardarson JH, Moore JE (2013) Quantum interference and Aharonov-Bohm oscillations in topological insulators. Rep Prog Phys 76:056501
31. Qu DX, Hor YS, Xiong J, Cava RJ, Ong NP (2010) Quantum oscillations and Hall anomaly of surface states in the topological insulator Bi_2Te_3. Science 329:821
32. Novoselov KS, Geim AK, Morozov SV, Jiang D, Katsnelson MI, Grigorieva IV, Dubonos SV, Firsov AA (2005) Two-dimensional gas of massless Dirac fermions in graphene. Nature 438:197

33. Gusynin VP, Sharapov SG (2005) Magnetic oscillations in planar systems with the Dirac-like spectrum of quasiparticle excitations. Phys Rev B 71: 125124
34. Hossain MZ, Rumyantsev SL, Shahil KMF, Teweldebrhan D, Shur M, Balandin AA (2011) Low-frequency current fluctuations in "graphene-like" exfoliated thin-films of bismuth selenide topological insulators. ACS Nano 5:2657
35. Goyal V, Teweldebrhan D, Balandin AA (2010) Mechanically-exfoliated stacks of thin films of Bi_2Te_3 topological insulators with enhanced thermoelectric performance. Appl Phys Lett 97:133117